In: ***Zeolites: Synthesis, Chemistry and Applications*** ISBN 978-1-61942-861-4
Editor: ANDREYEV, M. K; ZUBKOV, O. L., pp. 1-34

ZEOLITE FROM FLY ASH-IRON OXIDE MAGNETIC NANOCOMPOSITE: SYNTHESIS AND APPLICATION AS AN ADSORBENT FOR REMOVAL OF CONTAMINANTS FROM AQUEOUS SOLUTION

Denise A. Fungaro*, Mitiko Yamaura, Terezinha E. M. Carvalho, and José E. A. Graciano
Environment and Chemistry Centre, Nuclear and Energy Research Institute
(IPEN – CNEN/SP), São Paulo, Brazil

Abstract

This chapter presents and discusses current research on the study of the adsorption efficiency of zeolite from fly ash-iron oxide nanocomposites towards removal of hazardous pollutants from aqueous solutions. The magnetic properties of iron oxides have been combined with the adsorption features of zeolites synthesized from fly ash to produce a magnetic nanocomposite adsorbent. Magnetite nanoparticles in suspension were synthesized by precipitating iron ions in a NaOH solution. Zeolite was synthesized from coal fly ash by alkaline hydrothermal treatment. Zeolite-iron oxide composite was prepared by mixing zeolite with magnetite suspension with weight ratios of 3:1, 2:1 and 1:1. The resulting materials were characterized by X-ray diffraction, surface area, magnetization measurements, Fourier transform infrared and X-ray fluorescence analyses. Batch tests were carried out to investigate the adsorption mechanism of dyes and metal ions from aqueous solution onto magnetic nanocomposite. The composite adsorbents after be used to adsorb contaminants in water were removed from the medium by a simple magnetic process. The effect of various experimental parameters such as contact time, pH, adsorbent dose and temperature were investigated. The experimental data were analyzed using the pseudo-first-order, pseudo-second-order and intraparticle diffusion equations adsorption kinetic models. The Langmuir and Freundlich isotherm models were tested for their applicability. The results indicated that zeolite from fly ash-iron oxide magnetic nanocomposite**,** a low cost adsorbent**,** exhibited considerable potential for application in removal of contaminants from aqueous solution. Future prospects for research are discussed.

* E-mail address: dfungaro@ipen.br

1. INTRODUCTION

Magnetic separation technology as an efficient, fast and economical method for separating magnetic materials has been widely used in textile, biology and environmental protection [1–4]. Some examples of this technology are the use of magnetic poly(oxy-2,6-dimethyl1,4-phenylene) for the adsorption of organic dyes [5], polymer-coated magnetic particles for oil spill remediation [6], polyacrylic acid-bound iron oxide magnetic nanoparticles for the adsorption of methylene blue [7] and the use of montmorillonite–Cu(II)/Fe(III) oxide magnetic materials for the removal of humic acid [8].

Adsorption is an important technique for metals ion, color and any other pollutant removal from industrial wastewaters and radioactive wastes. The prediction of batch adsorption kinetics is necessary for the design of industrial adsorption columns.

The adsorbents combining magnetic separation technology with adsorption process have been widely used in environmental purification [9–11]. The main advantage of this technology is that it can dispose a mass of wastewater in a very short period of time and produce no contaminants such as flocculants [12]. After the adsorption is carried out, the adsorbent can be separated from the medium by a simple magnetic process.

Magnetic composites based on activated carbon/iron oxide, clay/iron oxide and NaY commercial zeolite/iron oxide have been prepared via a simple precipitation method and used for the removal of contaminants from aqueous effluents [13-15]. These materials possessed a high surface area and a high adsorption capacity.

The magnetized adsorbents have recently been used for removal of dyes from water [16].

Most commercially available magnetic particles are rather expensive and cannot be used large-scale processes. Magnetic modification of low cost adsorbents could lead to materials for biotechnology and environmental applications.

Fly ash is formed by combustion of coal in coal-fired power station as a waste product. The generation rate of coal fly ash in Brazil is approximately 4 million tons per year and is predicted to increase.

Great part of this fly ash is applied as raw material for cement and concrete production (~ 30% of the total), while a small part is used in road-stabilizer, glass composites and asphalt mixtures. The remaining solid wastes are disposed in on-site ponds, nearby abandoned or active mine sites, or landfills.

There is a big concern related to the non-use fly ash since is endangering surrounding surface and ground waters as it can release different and potentially toxic trace and major elements during and after its transport to the dump. Further on, leached elements are entering soils and sediments and through biosphere can enter food-chain. The coal ash in the environment is exposed to various influences, and solubilization processes take place, sometimes transforming almost insoluble metals to soluble species, and leading to pollution of water and soil [17–20].

Efficient disposal of coal fly ash is a worldwide issue due to its massive volume and harmful risks to the environment. Furthermore, the conversion of a low-cost waste product into a higher level product would make the disposal of the remaining unused ash far more economically viable. Thus continuous research is needed to develop an alternative technology for utilizing coal ashes. As a technique for recycling coal fly ash, synthesis of zeolites from coal fly ash has attracted a great deal of attention.

Holler and Wirsching [21] and Henmi [22] were the first to report the modification of fly ash by hydrothermal treatment in alkaline solutions at elevated temperatures and pressures to produce zeolites. Since them, the synthetic approach has been modified to include microwave assisted synthesis [23] and the fusion of ash with base prior to hydrothermal treatment [24].

Zeolitic materials have been widely used as low-cost adsorbents as reviewed by Querol et al. and Rayalu et al. [25, 26].

In our group we have been developing zeolites synthesized from Brazilian coal fly ashes to remove metals ions from aqueous effluents and soil. The efficiency of zeolitic materials as adsorbent allowed investigations focused on the removal of dyes [27-31].

In this study, the development of a new kind of magnetic adsorbent which can be effective for the removal of contaminants from aqueous solution was examined. For this purpose, the adsorption properties of zeolite synthesized from coal fly ashes were combined with the magnetic properties of iron oxides to produce zeolite-iron oxide magnetic composite. The adsorption studies such as effect of contact time, pH, adsorbent dose and temperature were explored in batch experiments and thermodynamic, kinetic and adsorption isotherm analyses were used to elucidate the adsorption mechanism.

2. MATERIALS AND METHODS

2.1. Materials

The sample of coal fly ashes from baghouse filter was obtained from a coal-fired power plant located at Figueira City, in Paraná State, Brazil. All chemicals used in this study were of analytical grade. Reactive Orange 16 (RO16; C.I. 17757; $C_{20}H_{17}N_3O_{10}S_3Na_2$; molar mass = 601.54 g mol^{-1}) was purchased from Sigma–Aldrich (50% purity) and Indigo Carmine (IC; C.I. 73015; $C_{16}H_8N_2Na_2O_8S_2$; molar mass = 466.35 g mol^{-1}) was supplied by Vetec Química Fina Ltda (100% purity). The standard solutions of metal ions Cd^{2+}, Pb^{2+} and Zn^{2+} were prepared from their salts (Merck). Stock solutions were prepared in deionized water (Millipore Milli-Q) and the solutions for adsorption tests were prepared by diluting. For pH adjustment, 0.01 mol L^{-1} HNO_3 and 0.5 mol L^{-1}NaOH were used.

2.2. Preparation of the zeolite from fly ash

Coal fly ash (CFA) was used as starting material for zeolite synthesis by means of hydrothermal treatment. In synthesis experiment, 20 g of fly ash was heated to 100 ^oC in an oven for 24 h with 160 mL of 3.5 mol L^{-1} NaOH solution. The zeolitic material was repeatedly washed with deionized water until pH 11 and dried at 50 ^oC for 12 h [22]. The zeolitic product obtained was labeled as ZFA.

2.3. Preparation of the zeolite-iron oxide magnetic nanocomposites

The composites were prepared using two different methods. In the first method, magnetite particles were prepared by adding of 2 mol L^{-1} NaOH solution drop by drop in a 100 mL solution of ferrous sulfate (1.8 g) with agitation until the pH reached 11. The slurry was heated on a water bath. After that, the magnetite was washed with distilled water and dried at room temperature. One part of the magnetite powder was separated and stored (MAG). Other part of magnetite particles was redispersed in aqueous solution and zeolite synthesized from fly ash (ZFA) was added slowly with agitation. The zeolite/magnetite ratio was 3:1 (w/w). The obtained zeolite-iron oxide magnetic composite was washed with distilled water, dried at room temperature and milled [30]. The magnetite composite obtained was labeled as ZM3.

In the second method, the composites were prepared by adding a 5 mol L^{-1} NaOH solution into a mixed solution of 0.25 mol L^{-1} ferrous chloride and 0.5 mol L^{-1} ferric chloride (molar ratio 1:2) until obtaining pH 11 at room temperature. The slurry was filtrated and washed repeatedly with distilled water until obtaining pH 7. Then particles were redispersed in aqueous solution and zeolite synthesized from fly ash (ZFA) was added. The amount of zeolite was adjusted in order to obtain zeolite/iron oxide weight ratios of 1:1, 2:1 and 3:1. The composites were filtrated and the obtained materials were dried in an oven at 50 ^{o}C [27]. The magnetic composites were named ZC1, ZC2 and ZC3 for the zeolite/iron oxide weight ratios of 1:1, 2:1 and 3:1, respectively.

Figure 1 show a photograph of the zeolite-iron oxide magnetic nanocomposites attracted toward the magnet.

Figure 1. Magnetic responses of the ZM3 (left) and ZC2 (right) in contact with a magnet.

2.4. Characterization techniques

The chemical composition of zeolite was determined by a RIX-3000 RIGAKU X-ray fluorescence spectrometer (XRF) equipped with a Rh X-ray tube (operated at 50 kV-60 mA). The surface area was determined by N_2 adsorption isotherm using NOVA 1200 (Quantachrome Corp.). Before adsorption experiments, the samples were degassed at 150 ^{o}C for 12 h. The specific surface area was obtained by five points at p/p^0 between 0.05 and 0.20 applying the Brunauer–Emmet–Teller equation to the adsorption data. Bulk density was determined by helium pycnometer (Micromeritics – Accupyc 1330). The phases of the zeolite were determined by X-ray diffraction analyses (XRD) with an automated Rigaku multiflex diffractometer with Cu anode using Co Kα radiation at 40 kV and 20mA over the range (2θ)

of 5–80^{o} with a scan time of 1^{o}/min. The images of scanning electron microscopy (SEM) were obtained using the scanning electron microscope Philips XL-30. Magnetization measurements were obtained at room temperature in magnetic fields up to 20 kOe using a vibrating sample magnetometer (Princeton Applied Research, model 4500). Fourier transform infrared (FTIR) spectra were recorded using KBr pellet technique on FTIR spectrometer Nicolet, Nesus 670.

2.5. Adsorption experiments

The adsorption capacity (mg g^{-1}) of adsorbents was calculated using the Eq. (1):

$$q_t = \frac{(C_0 - C_t)\,V}{M} \tag{1}$$

where q_t is the adsorbed amount of adsorbate per gram of adsorbent at any time t, C_0 and C_t the concentrations of the adsorbate in the initial solution and at any time t, respectively (mg L^{-1}); V the volume of the adsorbate solution added (L) and M the amount of the adsorbent used (g).

Through the following equation (Eq. (2)), it was possible to determine the extraction efficiency in the different experiments performed:

$$R\ (\%) = \left(\frac{C_o - C_t}{C_o}\right) 100 \tag{2}$$

where R is the efficiency of extraction or retention percentage, C_0 (mg L^{-1}) is the initial concentration of each adsorbate and C_t (mg L^{-1}) represents the concentration of the adsorbate at time t.

All the experiments, except the study of the influence of temperature, were carried out at laboratory ambient temperature, 298 ± 2 K.

2.5.1. Dye adsorption

The adsorption was performed using the batch procedure. The experiments were carried out by shaking 50 mg of adsorbent (ZM3) with 5 mL of dye solutions with initial concentration of 10.0 mg L^{-1} in a shaker operated at 360 rpm for 30-420 min in glass bottles. Samples were withdrawn at appropriate time intervals and placed on top of a magnet for 60 min to settle the particles and 4 ml of supernatant was taken for the measurement. The concentration of dye in the supernatant solution was analyzed using a UV spectrophotometer (Cary 1E – Varian) by measuring wavelength of maximum absorption at 493 nm for RO16 and 610 nm for IC. The same experiment was repeated with variations in some of the parameters such as: pH (2-10), mass of adsorbent (25-150 mg) and temperature (293-313 K). Each experiment was duplicated under identical conditions with maximum deviation was found to be 3%. For adsorption isotherms, samples with concentrations ranging from 1.2 to 20.0 mg L^{-1} for RO16 and 2.7 to 19.5 mg L^{-1} for IC were agitated till the equilibrium was achieved.

2.5.2. Heavy metal ion adsorption

Batch adsorption experiments were carried out by shaking 1 g of composite (ZC1, ZC2 or ZC3) with 100 mL of solutions containing metal ions. After shaking, the suspensions were placed on top of a magnet for 60 min to settle the particles and 25 mL of supernatant was taken for the measurement. The supernatant concentrations were determined by complexometric titration with EDTA. In kinetic studies, the contact time was 2, 4, 8, 15 and 24 h with concentrations in the range 260–520 mg L^{-1}. Adsorption isotherms of metal ions at initial concentrations in the range 260–1660 mg L^{-1} were determined after shaking the suspensions for 24 h. Each experiment was duplicated under identical conditions with maximum deviation was found to be 5%.

2.6. Kinetic models

A study of adsorption kinetics is desirable as it provides information about the mechanism, which is important for the efficiency of the process. It is important to be able to predict the rate at which contamination is removed from aqueous solutions in order to design an adsorption treatment plant.

The rate constants of the adsorbate removal from the solution by zeolite-iron oxide magnetic nanocomposites were determined using Lagergren pseudo-first-order (Eq. 3) and pseudo-second-order (Eq. 4) with linear form of equations as follows:

$$\log(q_e - q_t) = log - \frac{k_1 t}{2.303} \tag{3}$$

$$\frac{t}{q_t} = \frac{1}{k_2 q_e^2} + \frac{1}{q_e} t \tag{4}$$

where q_e is the amount of dye adsorbed at equilibrium (mg g^{-1}), qt is the amount of dye adsorbed at time t (mg g^{-1}), k_1 is the rate constant of the pseudo-first-order adsorption (min^{-1}), and k_2 is the rate constant of the pseudo-second-order kinetics (g mg^{-1} min^{-1}) [32, 33].

The possibility of intraparticle diffusion resistance affecting adsorption was explored using the appropriate intraparticle diffusion model as [34]:

$$q_t = k_{id} t^{\frac{1}{2}} + C \tag{5}$$

where k_{id} is the intraparticle diffusion rate constant (mg g^{-1} $min^{-0.5}$). According to Eq. (5), a plot of qt versus $t^{0.5}$ should be a straight line with a slope k_{id} and intercept C when adsorption mechanism follows the intraparticular diffusion process. Values of the C give an idea about the thickness of boundary layer, i.e., the larger the intercept is the greater the boundary layer effect.

2.7. Adsorption isotherms

The equilibrium adsorption isotherm is of importance in the design of adsorption systems. Several adsorption isotherm equations are available and two important isotherms are selected in this study, the Langmuir and Freundlich isotherms [35, 36].

The equilibrium data obtained in the present study were analyzed using the linear forms of the expressions of Langmuir (Eq (6)) and Freundlich (Eq (7)) isotherm models:

$$\frac{C_e}{q_e} = \frac{1}{Q_0 b} + \frac{C_e}{Q_0} \tag{6}$$

$$\log q_e = logK_F + \frac{1}{n}\, logC_e \tag{7}$$

where C_e is the equilibrium concentration (mg L^{-1}), q_e the amount adsorbed at equilibrium (mg g^{-1}), Q_0 is the maximum amount of adsorbate per unit weight of adsorbent to form a complete monolayer on the surface (mg g^{-1}); b is the Langmuir isotherm constant (L mg^{-1}), related to the affinity of the adsorption sites; K_F [(mg g^{-1}) (L $mg^{-1})^{1/n}$] and n are the Freundlich constants related to adsorption capacity and adsorption intensity of adsorbents, respectively.

The Langmuir isotherm can also be represented in terms of a dimensionless constant separation factor or an equilibrium parameter:

$$R_L = \frac{1}{1 + bC_o} \tag{8}$$

where b is the Langmuir constant (L mg^{-1}) and C_o the initial concentration of adsorbate (mg L^{-1}). R_L values between 0 and 1 indicate favorable adsorption [37]. The R_L is equal to the ratio of the unused adsorbent capacity to the maximum adsorbent capacity and thus it can be measurement of the adsorbent capacity used and the affinity between the adsorbate and adsorbent.

The non-linear regression Chi-square (χ^2) test was employed as a criterion for the fitting quality due to the inherent bias resulting from linearization of isotherm models. This statistical analysis is based on the sum of the squares of the differences between the experimental and model calculated data, of which each squared difference was divided by the corresponding data obtained by calculating from models [38]. The Chi-square can be represented by Eq. (9).

$$\chi^2 = \sum \frac{(q_e \exp - q_e calc)^2}{q_e calc} \tag{9}$$

where $q_e$exp is the equilibrium capacity of the adsorbent obtained from experiment (mg g^{-1}) and $q_e calc$ is the equilibrium capacity obtained by calculating from the model (mg g^{-1}). A low value of χ^2 indicates that experimental data fit better to the value from the model. Therefore, it is necessary to analyze the data set using the Chi-square test to confirm the best fit isotherm for the adsorption system combined with the values of the correlation coefficient.

3. RESULTS AND DISCUSSION

3.1. Dye adsorption studies

3.1.1. Kinetic studies

Fig. 2 shows the effect of contact time on the adsorption capacities of RO16 and IC by ZM3. It is clear that the adsorption capacity of ZM3 increased rapidly in the initial stages of contact time and gradually increased with prolonging the contact time until equilibrium. It can be seen that the adsorption equilibrium of RO16 and IC on ZM3 were reached at 300 and 360 min, respectively.

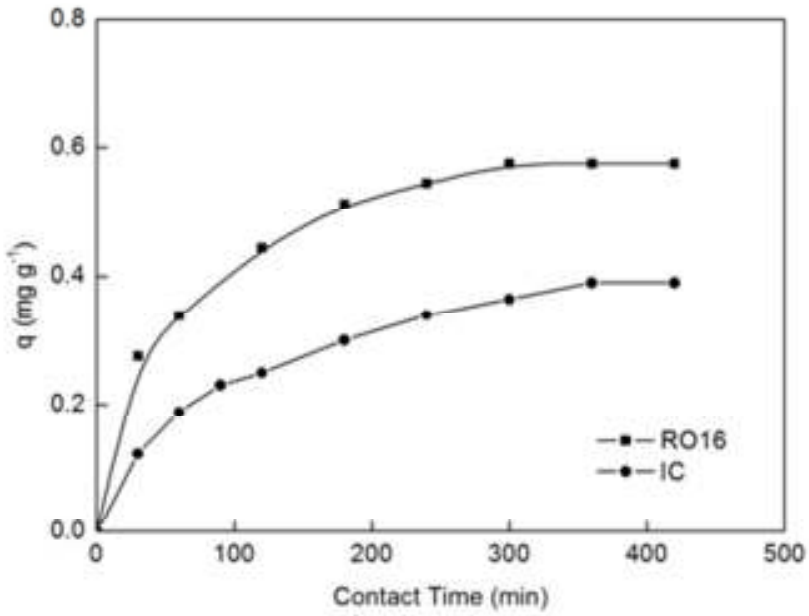

Figure 2. Effect of contact time on the adsorption of RO16 and IC by ZM3.

In order to investigate the adsorption processes of RO16 and IC by ZM3 pseudo-first-order (Eq. 3), pseudo-second-order kinetic (Eq. 4) and intraparticle diffusion (Eq. 5) models were used.

The calculated kinetic constants values and the corresponding linear regression correlation constants are given in Table 1. The pseudo second-order kinetic model better describes all of the dyes adsorption according to the correlation coefficients ($R_2 \geq 0.99$) than those of pseudo first-order model. In addition, the experimental adsorption capacity values were very close to the model-calculated adsorption capacity data (not shown), verifying the high correlation of adsorption to the pseudo-second-order model. The fitted linear regression plots of pseudo-second-order model are shown in Fig. 3.

Table 1. Kinetic parameters for the adsorption of dyes onto ZM3

Dyes	Pseudo-first-order			
	k_1 (min^{-1})	R_1		
RO16	1.15×10^{-2}	0.995		
IC	0.94×10^{-2}	0.973		
	Pseudo-second-order			
	k_2 (g mg^{-1} min^{-1})	h (mg g^{-1} min^{-1})	q_e (mg g^{-1})	R_2
RO16	3.90×10^{-2}	1.29×10^{-2}	0.659	0.999
IC	2.08×10^{-2}	0.470×10^{-2}	0.477	0.989
	Intraparticle diffusion			
	C (mg g^{-1})	k_i (mg g^{-1} $min^{-0.5}$)	R_i	
RO16	0.251	2.83×10^{-3}	0.956	
IC	0.037	1.87×10^{-2}	0.998	

The plots of intraparticle diffusion of RO16 and IC onto the ZM3 are illustrated in Fig. 4. The linearity of fitting lines in plots points to the presence of intraparticle diffusion. However, the deviation of the lines from the origin indicates that the pore diffusion is not the only rate controlling step [34, 39]. As the plot is often multilinear for many adsorption systems, it is common to segment it into two or more straight lines and to assume that different adsorption mechanisms control the step represented by each straight line [40]. Referring to RO16/ZM3 system, two distinct regions are observed (Fig. 4a). The first section of plots indicates that boundary layer diffusion probably limited dye adsorption. The second section shows the occurrence of intraparticle diffusion as the adsorption limiting step [41, 42].

The absence of such features in the plot of IC/ZM3 system (Fig. 4b) indicated that the steps were indistinguishable from one another and that the intraparticle diffusion was a prominent process right from the beginning of dye-solid interaction [43].

3.1.2. Adsorption isotherms

The isotherm parameters for RO16 and IC of two models are presented in Table 2. The isotherms of the two dyes with the experimental data points and the two theoretical isotherms plotted on the same graph are given in Fig. 5.

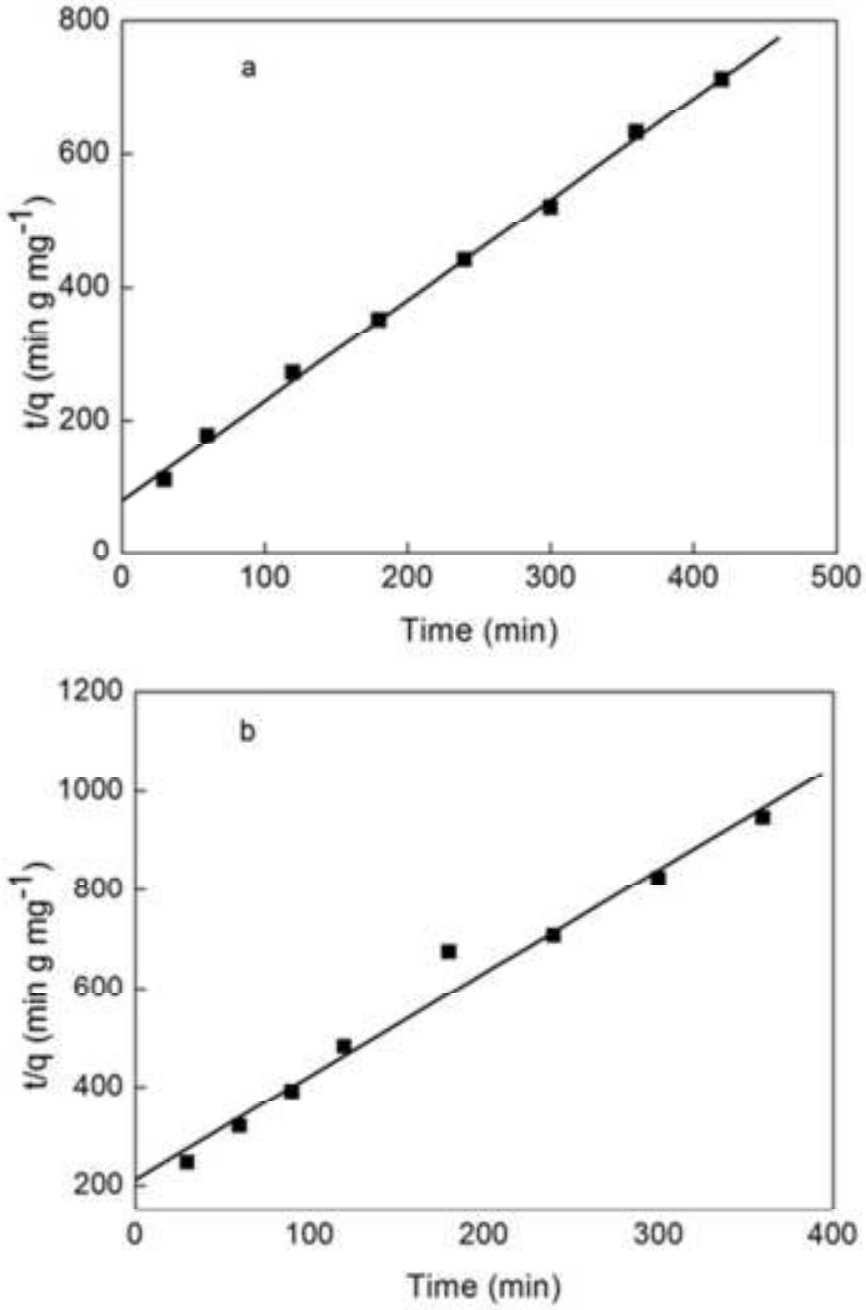

Figure 3. Pseudo-second-order adsorption kinetics of (a) RO16, (b) IC on ZM3.

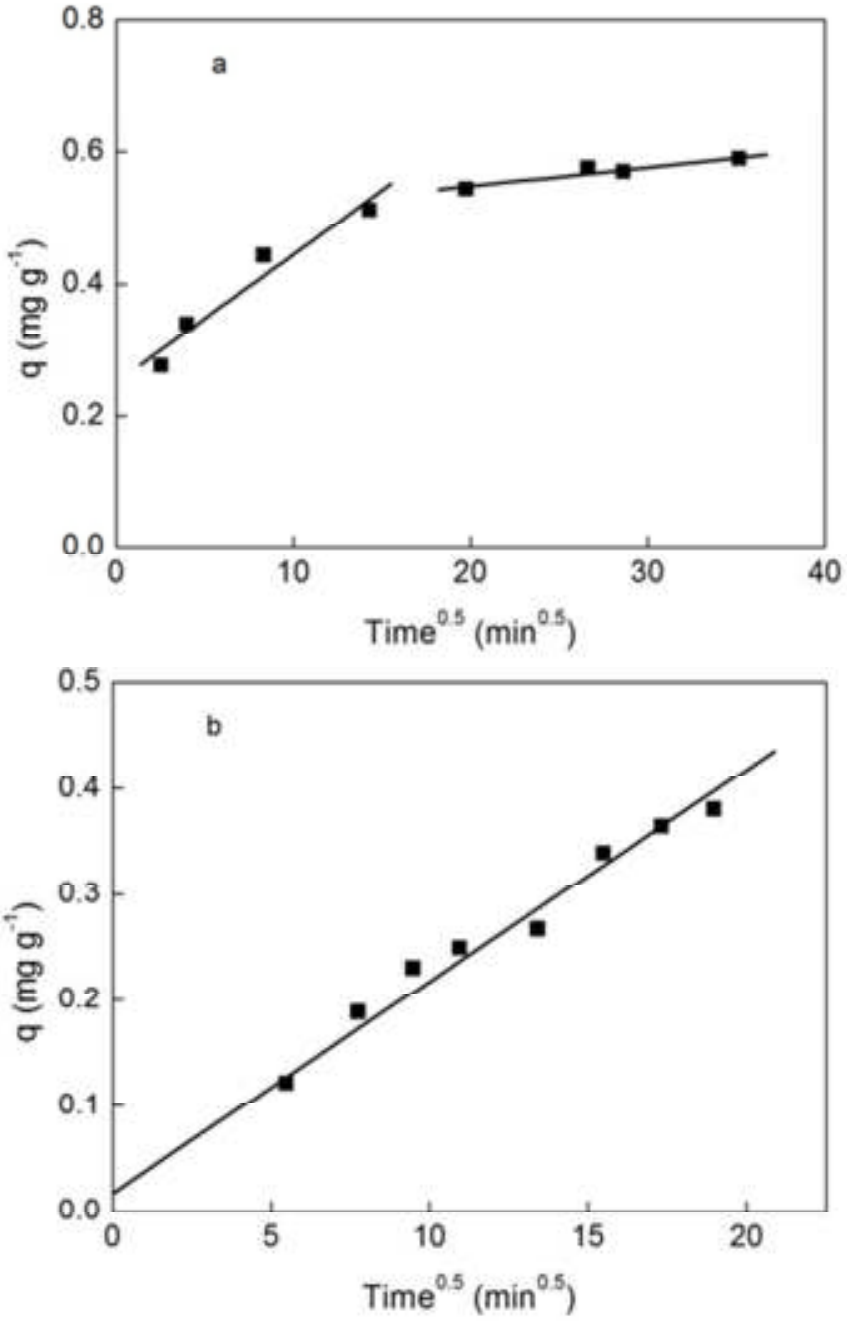

Figure 4. Intraparticle diffusion model of (a) RO16, (b) IC on ZM3.

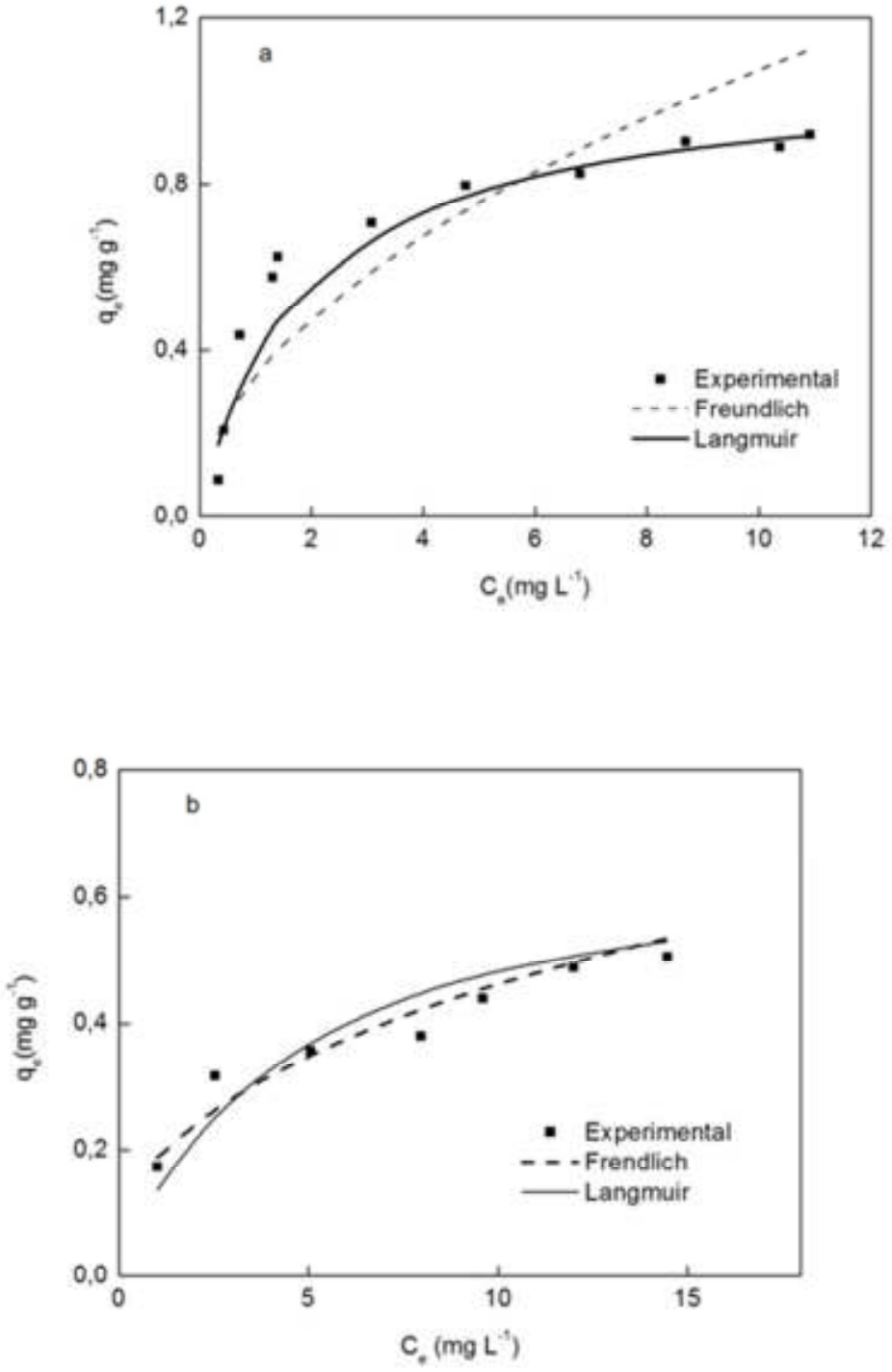

Figure 5. Adsorption isotherms of dyes onto ZM3: (a) RO16; (b) IC.

Table 2. Langmuir and Freundlich parameters for the adsorption of RO16 and IC onto ZM3

Dye	Langmuir			
	Q_o (mg g^{-1})	b (L mg^{-1})	R	χ^2
RO16	1.06	0.582	0.984	0.169
IC	0.583	0.359	0.988	0.0382
	Freundlich			
	K_f [(mg g^{-1}) (L $mg^{-1})^{1/n}$]	n	R	χ^2
RO16	0.340	2.00	0.874	0.452
IC	0.191	2.68	0.972	0.0161

The Langmuir isotherm gave a better fit than the Freundlich isotherm by giving greater R value closer to unity (0.98) and smaller value of χ^2 for RO16 adsorption by ZM3. For IC, the correlation coefficients for the Freundlich model and the Langmuir model are much similar but according to the χ^2 values, the best-fit isotherm model was the Freundlich isotherm model [38]. The value of n, which is significantly higher than unity, indicated that both RO16 and IC dyes are favourably adsorbed by zeolitic material for under the experimental condition [44].

In general for the adsorption process, the degree of adsorption depends on both the active sites of the adsorbent and the adsorbate properties. An interaction occurs between active sites on zeolite-iron oxide magnetic nanocomposite (Si-O and O-H) and SO_3^-, –N=N– and -N=C– -C=C– groups and aromatic skeletal vibrations of dyes [41, 45, 46].

3.1.3. Effect of solution pH

The pH was shown to be an important parameter in terms of the adsorption capacity, influencing not only the surface charge of the adsorbent but also the level of ionization of the material present in the solution. The effect of initial pH values for the adsorption of RO16 and IC dyes in solution onto ZM3 was investigated in the range of pH 2.0–10.0 (Fig. 6).

The adsorption of RO16 dyes on ZM3 is controlled by a pH-independent adsorption mechanism. The fact that the adsorption of dye onto zeolite from fly ash composite is not significantly affected with changing of initial pH of the dye solution may be attributed to the weak electrostatic interaction between the dye molecules and the sites on the surface of the zeolite particles [47] and neither the chemical species present in solution nor the effects of pH on the material superficies are important parameters for the adsorption processes.

It can be seen that the adsorption of IC was pH-dependent (Fig. 6). The amount adsorbed decreased as pH decreased from 2 to 4 and from 10 to 8 and remained constant in the pH interval between 4 to 8. The chemical species has an important effect on the adsorption of indigo carmine on the magnetic composite. Indigo carmine may undergo a redox process involving the uptake of one proton per electron transferred or two protons per two electrons transferred. Transfer of the second electron results in formation of the hydroquinone [48]. These results may indicate that the species present interacts with the adsorbent and the interactions between IC and composite surface can occurs due electrostatic force and weak

interaction of van der Walls forces. Previous studies have demonstrated that another possible interaction mechanism of the IC with magnetic zeolitic material composite is catalytic degradation [48, 49].

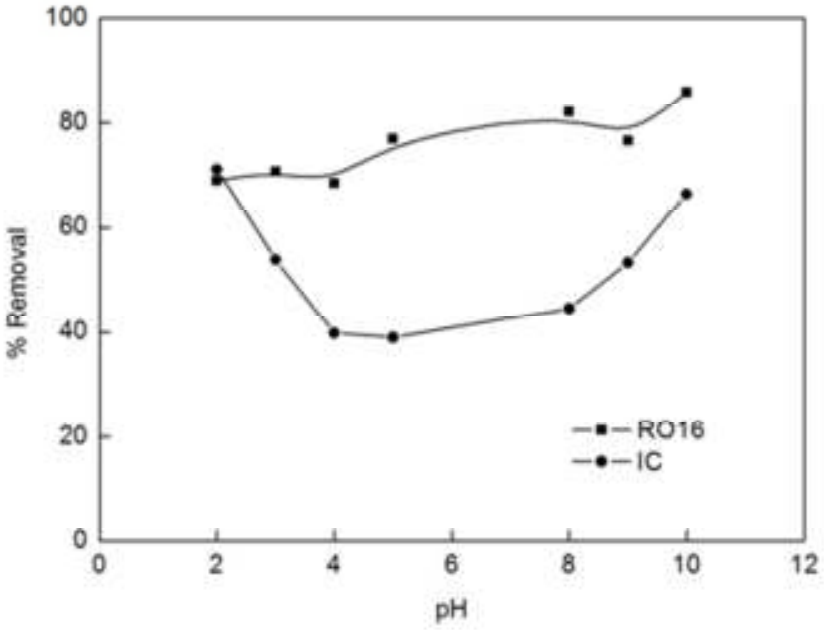

Figure 6. Effect of initial solution pH on dyes removal.

3.1.4. Effect of adsorbent dosage

The study of adsorbent mass for the removal of dyes from aqueous solution was carried out using adsorbent masses ranging from 25 to 150 mg of ZM3 and fixing the initial dye concentration (Fig. 7).

The highest amount of dye removal was attained for adsorbent mass of 100 mg for RO16 (Fig. 7a). For adsorbent dosages higher than this value, the percentage of dye removal remained almost constant. The increases in the removal efficiency with the adsorbent dose can be attributed to increase surface area and the availability of more adsorption sites as already reported in several papers [50, 51].

On the other hand, the increase in the adsorbent masses promoted a remarkable decrease in the amount of RO16 uptake per gram of adsorbent (q_e). The drop in adsorption capacity is basically due to sites remaining unsaturated during the adsorption and particle aggregation [52, 53]. This effect can be also mathematically explained by combining of equations [54].

For IC, along with the increase of adsorbent dosage from 25 to 150 mg, the percentage of dye removal increased and the adsorption capacity (q_e) decreased after 100 mg (Fig. 7b).

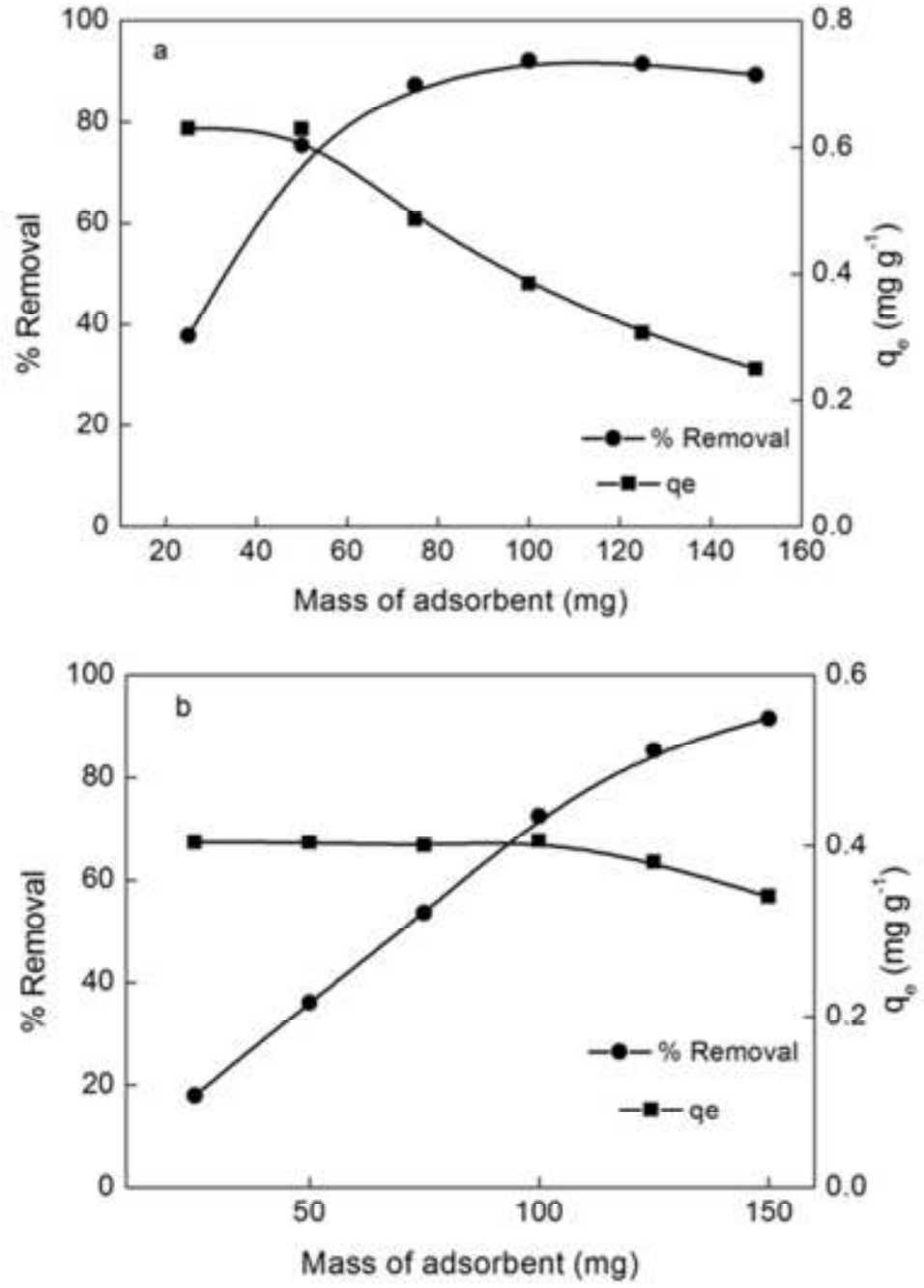

Figure 7. Effect of adsorbent mass on the percentage of removal and amount of dye adsorbed on ZM3: (a) RO16; (b) IC.

3.1.5. Effect of temperature

As the temperature can influence the final value of adsorption, the study of its effects on the adsorption process becomes an important aspect in waste water treatment. The variation was explained on the basis of thermodynamic approach. The thermodynamic parameters, ΔG^o, ΔH^o and ΔS^o, were calculated with the help of following Eqs. (10)-(13):

$$K_C = \frac{C_A}{C_S} \tag{10}$$

$$\Delta G° = -2{,}303RT\ logK_C \tag{11}$$

$$\Delta H° = 2{,}303R\left(\frac{T_1T_2}{T_2 - T_1}\right) log\ \frac{K_{C2}}{K_{C1}} \tag{12}$$

$$\Delta S° = \frac{\Delta H° - \Delta G°}{T} \tag{13}$$

where C_A is the equilibrium concentration of the adsorbate ions on adsorbent (mg L^{-1}); C_S is the equilibrium concentration of the adsorbate ions in the solution (mg L^{-1}); R is the gas constant, T is temperature on the absolute scale and K_C, K_{C1}, and K_{C2} are the equilibrium constants at temperature T, T_1 and T_2, respectively.

The values of these parameters were calculated and are presented in Table 3. The values of ΔG^o of dye/ZM3 adsorption systems are all negative, which indicates the spontaneous adsorption processes. Moreover, the increase in the absolute value of ΔG^o with increasing temperature indicates that higher temperatures facilitated the adsorption. The positive value of ΔH^o indicates that the adsorptions of both dyes onto ZM3 are endothermic. The positive value of ΔS^o suggests that in the dye/ZM3 adsorption systems, although the adsorption process caused an entropy decrease for the adsorbed dye molecules, the entropy increase of dye molecules in dissolved state due to rising temperature was much greater, and consequently the ΔS^o of the whole adsorption system increased.

Table 3. Thermodynamic parameters for adsorption of both dyes onto zeolite from fly ash-iron oxide magnetic nanocomposite

Dye	T (K)	ΔG^o (kJ mol^{-1})	ΔH^o (kJ mol^{-1})	ΔS^o (J $K^{-1}mol^{-1}$)
RL16	298	-0.71	74.0	251
	303	-1.96	13.2	50.2
	313	-2.46		
IC	298	-0.44	1.83	7.60
	303	-0,47	22.7	76.4
	313	-1.24		

3.2. Adsorption studies of Zn^{2+} ions onto zeolite-iron oxide magnetic nanocomposites

3.2.1. Adsorption isotherms

Adsorption isotherms were determined for the adsorption of Zn^{2+} ions onto pure zeolite (ZFA) and zeolite/Fe oxide composites (ZC1, ZC2 and ZC3). The results are shown in Fig. 8. The adsorption capacities increased with increasing equilibrium Zn^{2+} concentrations and eventually attained a plateau value.

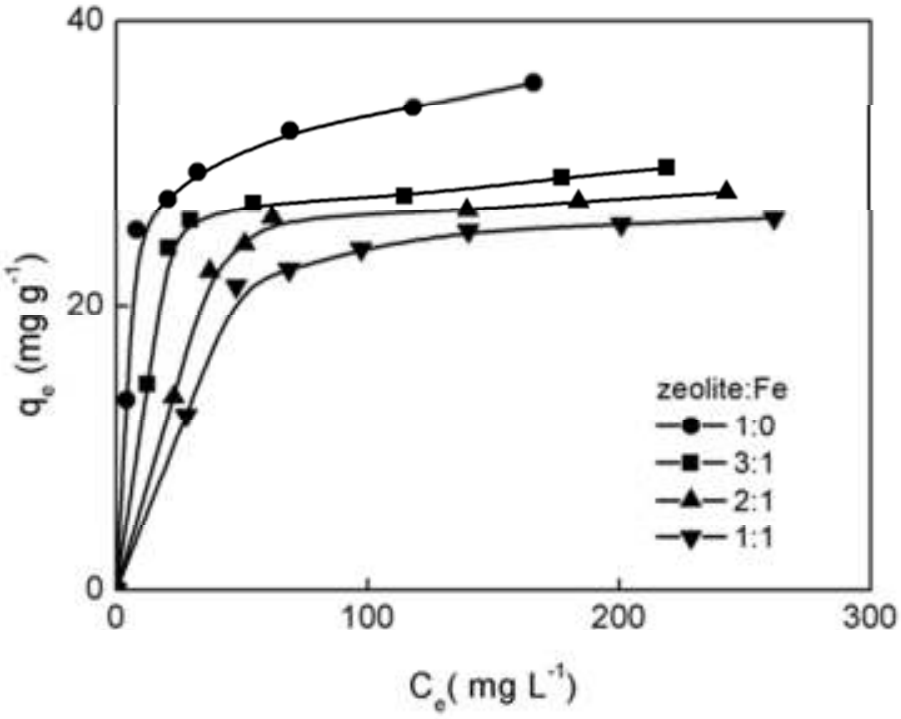

Figure 8. Equilibrium adsorption isotherms for Zn^{2+} ions onto pure zeolite and zeolite/Fe oxide composites 3:1, 2:1 and 1:1.

The adsorption capacity for the Zn^{2+} decreases in the order zeolite > 3:1 composite > 2:1 composite > 1:1 composite. It is interesting to note that the presence of the iron oxide does not significantly affect the adsorption capacity of the zeolite on the composites. The lower adsorption capacity of the composites is probably related to the decrease in surface area caused by the presence of the iron oxide. Similar results were obtained for the adsorption of Zn^{2+} on clay/iron oxide composites [15].

The isotherm shapes are largely determined by the adsorption mechanism and can therefore be used to diagnose the nature of the adsorption [55]. The adsorption isotherm for solution may be classified into four main classes relating to their shapes termed S, L, H and C and subgroups 1, 2, 3, 4 or max. Figure 8 clearly shows that adsorption isotherms are L2 type.

In L2-type isotherms, adsorption of solute on the adsorbent proceeds until a monolayer is established, with the formation of more than one layer not being possible.

Figures 9 and 10 depict linear Langmuir and Freundlich plots for the adsorption of Zn^{2+} ions onto pure zeolite and zeolite/Fe oxide composites, respectively. The isotherm constants and correlation coefficients calculated for Freundlich and Langmuir equations are given in Table 4.

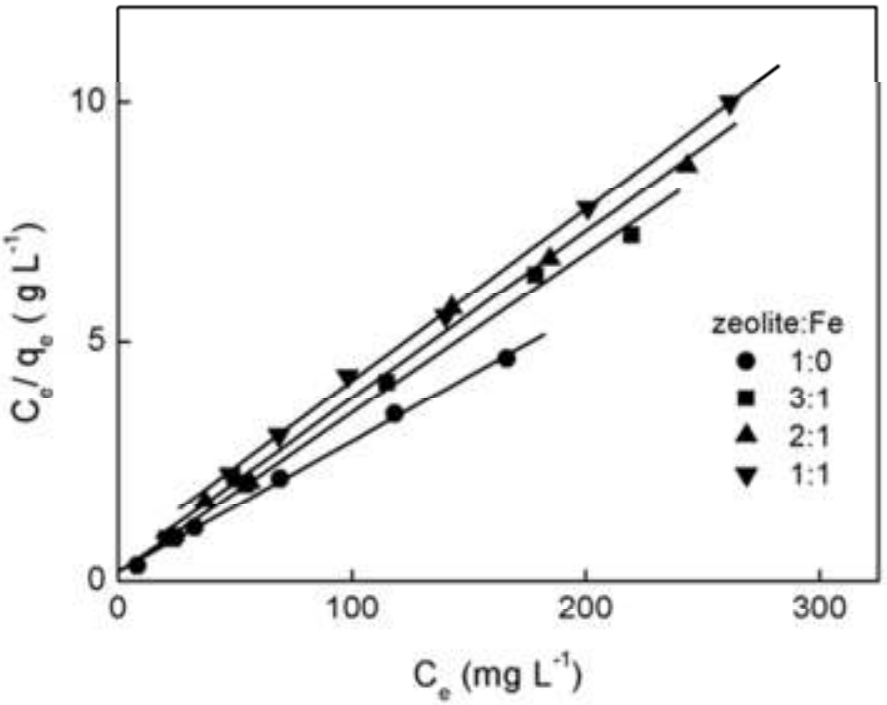

Figure 9. Langmuir plots for the adsorption of Zn^{2+} ions onto pure zeolite and zeolite/Fe oxide composites.

Table 4. Langmuir and Freundlich parameters for the adsorption of Zn^{2+} ions onto pure zeolite and zeolite/Fe oxide composites

Adsorbent	Langmuir Q_o (mg g^{-1})	b (L mg^{-1})	R_L	R^2
Zeolite:Fe 1:1	27.8	0.062	0.668	0.999
Zeolite:Fe 2:1	28.6	0.108	0.536	0.998
Zeolite:Fe 3:1	30.0	0.175	0.417	0.998
Zeolite	36.8	0.113	0.016	0.999
	Freundlich K_f *	n	R^2	
Zeolite:Fe 1:1	53.4	8.75	0.869	
Zeolite:Fe 2:1	17.8	12.4	0.737	
Zeolite:Fe 3:1	21.1	16.5	0.824	
Zeolite	19.3	8.42	0.983	

(*)[(mg g^{-1})(L mg^{-1})$^{1/n}$]

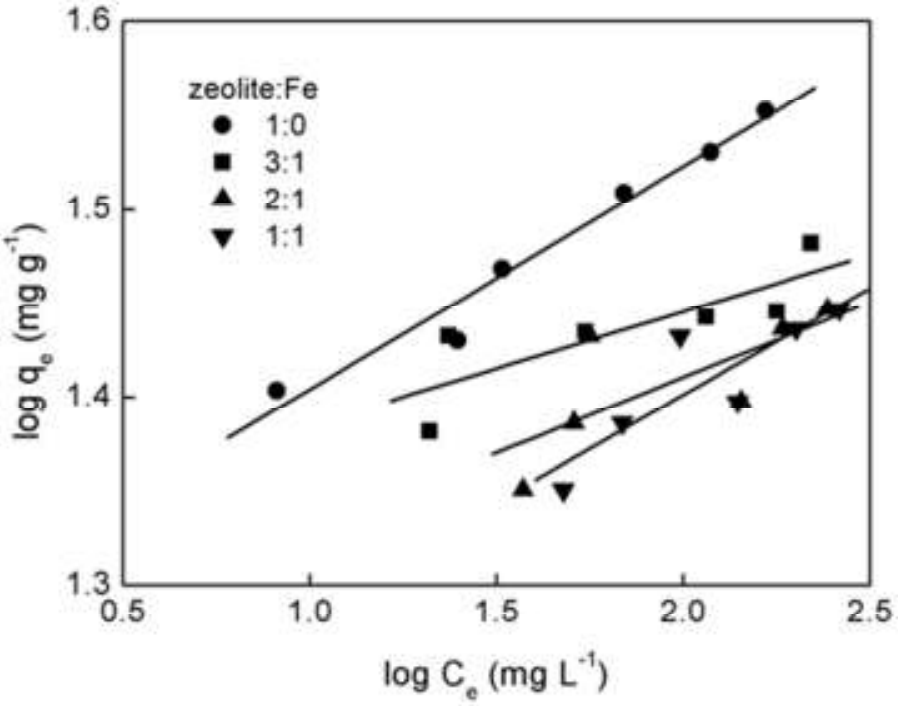

Figure 10. Freundlich plots for the adsorption of Zn^{2+} ions onto pure zeolite and zeolite/Fe oxide composites.

It can be observed from the Table 4 that the according the correlations coefficients criterion (R^2), the Langmuir model fits the experimental data better than the Freundlich model. The calculated R_L values were between 0 and 1 at all the adsorbents studied indicating the favorable condition for adsorption process.

The 2:1 zeolite-iron oxide nanocomposite (ZC2) was chosen for the studies of kinetic, thermodynamic characteristics and adsorption process of Cd^{2+} and Pb^{2+} from aqueous solution.

3.2.2. Effect of contact time and initial concentration

Figure 11 shows the effect of initial Zn^{2+} concentration at different contact time on adsorption of ZC2. The results showed that the extent of adsorption increased rapidly in the initial stages before 5 h and then approaches equilibrium after 10 h.

During the initial stage of adsorption, a large number of vacant surface sites are available for adsorption. After lapse of some time, the remaining vacant surface sites are difficult to be occupied due to repulsive forces between the solute molecules on the solid surface and the bulk phase. Besides, the metal ions are adsorbed into the pores that get almost saturated with metal ions during the initial stage of adsorption. Thereafter, the metal ions have to traverse farther and deeper into the pores encountering much larger resistance. This results in the slowing down of the adsorption during the later period of adsorption.

An increase in the initial Zn^{2+} concentration leads to an increase in the adsorption capacity of the Zn^{2+} on composite. The initial concentration provides an important driving

force to overcome all mass transfer resistances of the ion between the aqueous solution and solid phases. Hence a higher initial concentration of ion enhances the sorption process.

The time to reach equilibrium was independent of initial Zn^{2+} concentration. The adsorption of Zn^{2+} decreased from 86 to 54% by increasing Zn^{2+} concentration from 260 to 520 mg L^{-1}. The increase in initial Zn^{2+} concentration results in the fast attainment of saturation of composite and higher residual Zn^{2+} in the equilibrium solution. Further, it was observed that removal curves are single, smooth and continuous suggesting the formation of monolayer of adsorbate on the surface of the adsorbent [56].

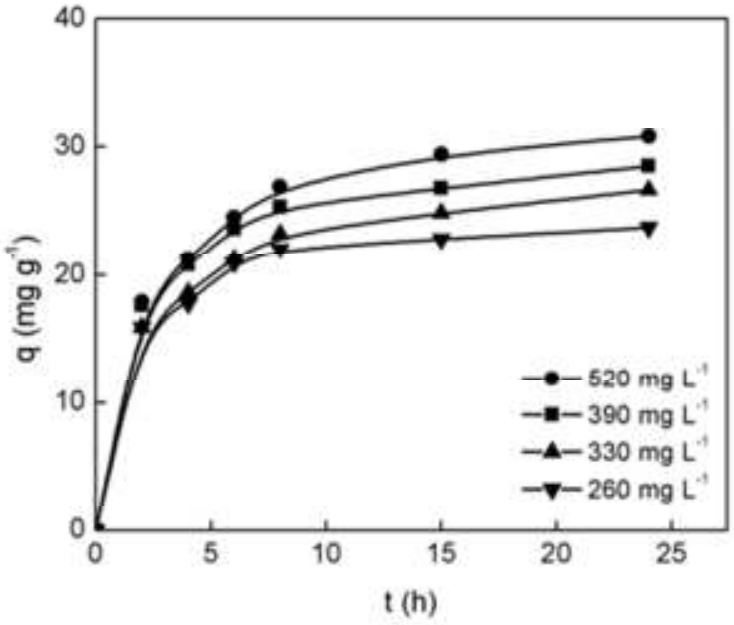

Figure 11. Adsorption kinetics for Zn^{2+} onto zeolite/iron oxide (2:1) composite.

3.2.3. Kinetic models

Figures 12-14 present the plots for the adsorption of Zn^{2+} on zeolite/iron oxide (2:1) using the pseudo-first-order kinetics, pseudo-second-order kinetics and intraparticle diffusion model. The calculated kinetic constants values and the corresponding linear regression correlation constants are given in Table 5.

As seen in Table 5, the correlation coefficients values obtained from pseudo-second-order kinetic were found to be higher than for the pseudo-first-order and intraparticle diffusion models. Kinetic studies on adsorption of composite for Zn^{2+} ions by using the pseudo-second-order rate expression provided the best fitting kinetic model.

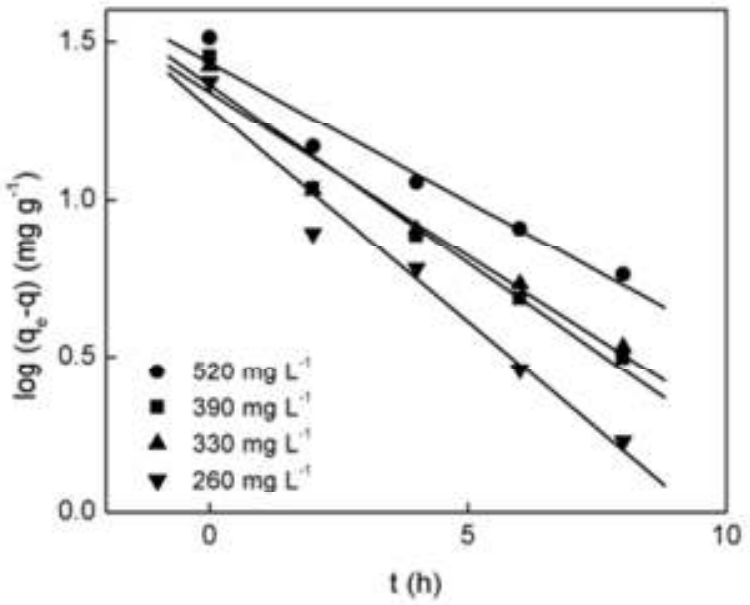

Figure 12. Pseudo-first-order kinetic plot for Zn^{2+} onto zeolite/iron oxide (2:1) composite.

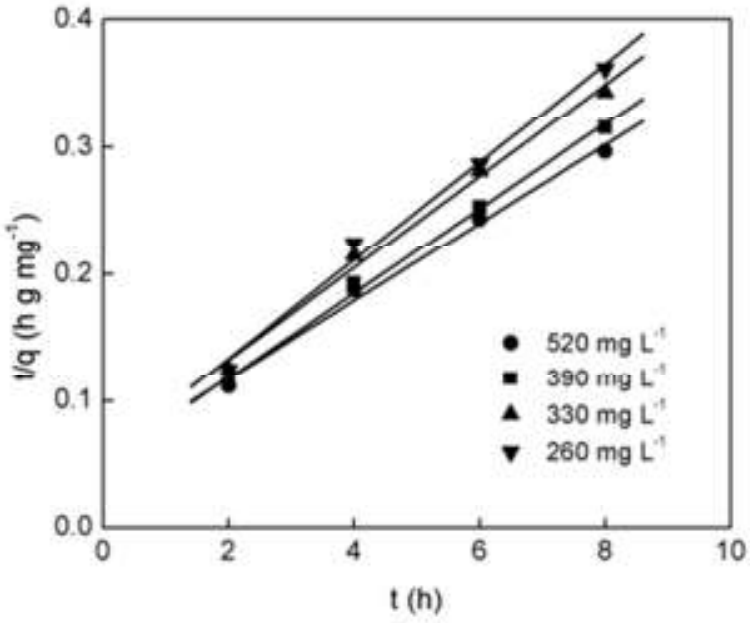

Figure 13. Pseudo-second-order kinetic plot for Zn^{2+} onto zeolite/iron oxide (2:1) composite.

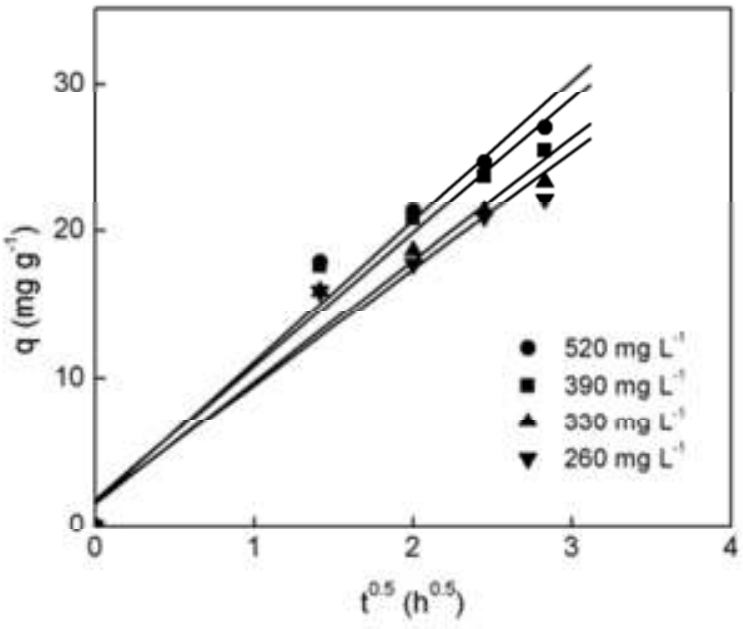

Figure 14. Intraparticle diffusion plot for Zn^{2+} onto zeolite/iron oxide (2:1) composite.

Table 5. Kinetic constants for Zn^{2+} onto zeolite/iron oxide (2:1) composite

[Zn] (mg L^{-1})	Pseudo- first-order			
	K_1 (h^{-1})	R_1^2		
260	3.14 x 10^{-1}	0.984		
330	3.34 x 10^{-1}	0.979		
390	2.61 x 10^{-1}	0.980		
520	2.04 x 10^{-1}	0.976		
	Pseudo- second-order			
	K_2 (g mg^{-1} h^{-1})	h (mg g^{-1} h^{-1})	q_e (mg g^{-1})	R_2^2
260	2.62 x 10^{-2}	0.176	25.9	0.995
330	2.14 x 10^{-2}	0.164	27.7	0.996
390	2.18 x 10^{-2}	0.193	29.8	0.998
520	0.164 x 10^{-2}	1.76	32.6	0.996
	Intraparticle diffusion			
	C (mg g^{-1})	K_i (mg g^{-1} $h^{-0.5}$)	R_i^2	
260	1.68	7.86	0.974	
330	1.53	8.23	0.981	
390	1.78	9.04	0.979	
520	1.58	9.53	0.985	

For the diffusion model plots (Fig. 14), the linearity of the fitting lines points the presence of intraparticle diffusion. However, the deviation of the lines from the origin indicates that although intraparticle diffusion was involved in the adsorption process, it was not the rate-controlling step [34].

3.2.4. Evaluation of thermodynamic parameters

The adsorption of Zn^{2+} from solutions aqueous on the zeolite/iron oxide (2:1) composite at different temperatures was studied. The values of standard free energy (ΔG^o), enthalpy (ΔH^o) and entropy (ΔS^o) were calculated (Eqs 10-13) and are presented in Table 6.

Table 6. Thermodynamic parameters for adsorption of Zn^{2+} on zeolite/iron oxide (2:1) at different temperatures

Temperature (K)	ΔGº (kJ mol^{-1})	ΔHº (kJ mol^{-1})	ΔSº (J K^{-1} mol^{-1})
298	-3.90	6.42	34.6
303	-4.07	47.8	171
313	-5.78		

It is obvious from this table that the negative and small values of free energy change (ΔG^o) were an indication of spontaneous nature of the adsorption process. The positive values of standard enthalpy change (ΔH^o) at different temperatures were indicating the endothermic nature of the adsorption process. The positive values of (ΔS^o) suggested the increased randomness at the solid/solution interface during the adsorption of the zinc onto composite.

3.3. Adsorption isotherms of Pb^{2+} and Cd^{2+} on 2:1 zeolite/iron oxide composite

The adsorption isotherms of Pb^{2+} and Cd^{2+} on 2:1 zeolite/iron oxide composite (ZC2) are shown in Fig. 15. The isotherm of Zn^{2+} is plotted on the same graph for comparison of results. The shape of isotherms are of ‘‘L2’’ type according to Giles classification for isotherms [55]. This shape indicated that the data have reached a maximum value, resulting in the presence of the plateau. L-isotherm type (or Langmuir isotherm type) is usually associated with ionic substrates (e.g., metal cations) adsorption with weak competition from the solvent molecules.

The Q_o, b, K_f, n values and the linear regression correlations (R^2) for Langmuir and Freundlich are listed in Table 7. Based on these data, it showed that the Langmuir isotherm fitted the data better with regression coefficients $R^2 > 0.99$. The R_L values shown were $0 < R_L < 1$ suggesting the favorable adsorption isotherm of metals onto ZC2.

Using the Langmuir model, the maximum adsorption capacity for the metals can be estimated as: $Pb^{2+} > Cd^{2+} > Zn^{2+}$. The same order of selectivity obtained with zeolite-from fly ash-iron oxide composite was determined with natural zeolites and is related to the characteristics of the metal ions [57, 58].

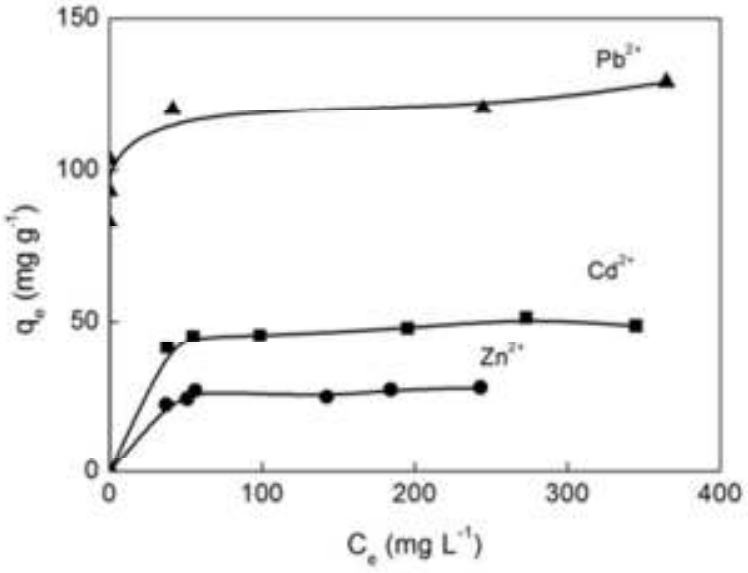

Figure 15. Adsorption isotherms of Pb^{2+}, Cd^{2+} and Zn^{2+} on 2:1 zeolite/iron oxide composite.

Table 7. Langmuir and Freundlich parameters for the adsorption of metal ions onto 2:1 zeolite/iron oxide composite

Adsorbate	Langmuir			
	Q_o (mg g^{-1})	b (L mg^{-1})	R_L	R^2
Zn^{2+}	28.5	0.108	0.536	0.998
Cd^{2+}	50.8	0.114	0.147	0.999
Pb^{2+}	127	0.657	0.917 x 10^{-3}	0.999
	Freundlich			
	K_f*	n	R^2	
Zn^{2+}	17.8	12.4	0.737	
Cd^{2+}	31.7	12.7	0.918	
Pb^{2+}	109	41.7	0.674	

(*)[(mg g^{-1})(L mg^{-1})$^{1/n}$]

The selectivity could be the result of various factors which influence ion-exchange behavior in zeolites. The specificity of a surface containing fixed charges for metal ions can be accounted for in terms of ion hydration and electrostatic bond energies [59, 60].

The metal ions with higher electronegativity adsorb more readily and the obtained selectivity series is in agreement with the metal ions electronegativity, namely Pb^{2+} (2.33) > Cd^{2+} (1.69) > Zn^{2+} (1.65) [61]. Also, the differential adsorption of metal ions may be ascribed to the difference in their ionic radii. The smaller the ionic radius, the greater its tendency to hydrolyze leading to reduced adsorption. The ionic radii of Pb^{2+}, Cd^{2+} and Zn^{2+} are 1.21 Å, 0.97 Å and 0.74 Å, respectively [61].

The adsorption process of metal cations by zeolites has been extensively studied [62]. Most studies considered it as a cation exchange process between metal cations presence in water and cations in the zeolite framework. Researchers also proposed the adsorption of metal cations was due to the surface reaction with terminal hydroxyl groups on zeolites and the combination of positive charges of metal cations and negative charges on zeolite surfaces. Metal removal is often accomplished by precipitating, particularly at high initial metal ion concentrations.

4. CHARACTERIZATION OF MATERIALS

4.1. Physicochemical properties

Table 8 shows some properties of coal fly ash (CFA), zeolite from fly ash (ZFA) and zeolite/Fe oxide composites (ZM3 and ZC2). The chemical compositions and BET results suggested that CFA was partly converted into zeolitic products. The chemical composition of materials is mainly silica, alumina and iron oxide. A significant amount of Na element is incorporated in the zeolitic product ZFA due the hydrothermal treatment with NaOH solution.

The inclusion of magnetite during synthesis of composite ZM3 does not seem to affect the BET area of the zeolite (there is a perceptible decrease, from 53 to 51, but it must be taken into account that in the composite sample one quarter of the weight corresponds to magnetite). The fact that the surface area is roughly maintained indicates that most of the pore mouths of the zeolitic channels remain open after the inclusion of magnetite. The value of surface area of the composite prepared via iron chloride ions co-precipitation method (ZC2) was much higher than that of zeolitic material (ZFA). This is probably related to the porous texture of the formed iron oxide contributing for the increase of the surface area and microporosity.

Colors of iron oxide are very dependent on grain size and chemical composition and this feature is a first auxiliary attribute in their identification. The ZM3 was black suggesting the presence of pure magnetite while the ZC2 was brownish product, indicating a mixture of two iron oxides, magnetite and maghemite.

4.2. X-ray diffraction analysis

XRD patterns of samples are shown in Fig. 16. It can be seen that the peaks in the synthesized magnetite MAG, Fe_3O_4, are in agreement with the data of the face-centered cubic (fcc) of the reported pattern of reference magnetite in the ICDD nº 19-629. All MAG peaks showed broad diffraction lines and well defined peaks indicating that the crystallites were very small.

The XRD analyses of all zeolitic materials showed that hydroxysodalite (ICDD 00-011-0401) was the major zeolitic phase with peaks of quartz (ICDD 001-0649) and mullite (ICDD 002-0430) of fly ash that remained after the alkaline hydrothermal treatment.

The obtained zeolite from coal fly ash (ZFA) showed crystalline components no peaks of magnetite indicating the absence of same in accordance with the composition of the material.

Table 8. Chemical compositions and textural properties of materials

	CFA	ZFA	ZM3	ZC2
SiO_2	27.7	23.9	11.08	9.8
Al_2O_3	9.1	10.8	4.6	4.4
Fe_2O_3	39.8	48.3	77.8	80.2
K_2O	9.4	2.2	0.80	0.85
CaO	4.0	4.9	2.1	1.6
TiO_2	3.0	3.7	1.2	0.96
ZnO	1.7	1.6	0.43	0.44
As_2O_3	1.4	0.09	0.09	0.09
SO_3	1.3	1.1	0.44	0.31
MgO	0.46	0.51	0.17	0.20
PbO	0.44	0.51	0.16	0.16
U_3O_8	0.30	0.35	0.35	0.35
Na_2O	0.22	0.86	0.33	0.28
MnO	0.21	0.25	0.14	0.14
ZrO_2	0.15	0.19	0.04	0.03
SrO_2	0.13	0.16	0.16	0.02
P_2O_5	0.13	0.08	0.44	0.44
Cr_2O_3	0.13	0.10	0.10	0.03
Rb_2O	0.10	0.03	0.03	0.03
NiO	0.09	0.13	0.11	0.05
GeO_2	0.07	0.03	0.03	0.03
CuO	0.07	0.08	0.08	0.08
Ga_2O_3	0.05	0.02	0.02	0.02
S_{BET} (m^2/g)	10.6	53.0	51.0	78.2
Bulk density (g/cm^3)	2.40	2.54	2.96	2.96

The crystallite size (D) of magnetite particles for samples of MAG, ZM3 and ZC2 was estimated from the X-ray diffraction peak (311) using the Scherrer formula [63] represented by the Equation 14. The Scherrer equation is limited to nano-scale and is given for particles of spherical shape (shape factor of typical value 0.9). In this work in order to apply the Scherrer formula the spherical shape of nanoparticles was considered.

$$D = \frac{0.9\,\lambda}{\beta_{1/2} cos\theta} \tag{14}$$

where λ is the wavelength of the X-ray source ($Cu_{K\alpha 1}$), $\beta_{1/2}$ is the angular width at the half maximum intensity of the diffraction peak (rad) and θ is the Bragg angle.

The estimated crystallite size of magnetite of the samples are given in Table 9. As can be seen the crystallite is nanosize, which may be smaller or equal to the grain size. The nanoparticles are also evidenced in the XRD pattern by broad peaks and distinct. The magnetite prepared via iron chloride ions co-precipitation method present in the ZC2 composite showed crystallite size smaller than the ZM3 composite.

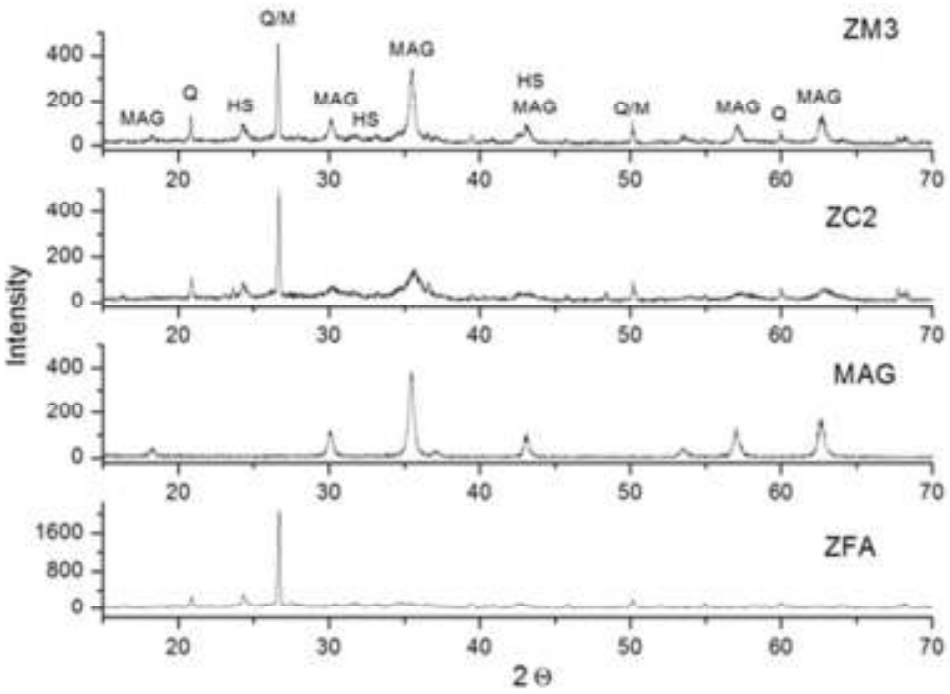

Figure 16. X-ray diffractograms for zeolite from fly ash (ZFA), magnetite (MAG) and zeolite/Fe oxide composites (ZM3 and ZC2). M = mulitte; Q = quartz; MAG = magnetite; HS = hydroxysodalite.

Table 9. XRD crystallite size of the samples of MAG, ZM3 and ZC2 for the (311) peak of magnetite

sample	MAG	ZM3	ZC2
crystallite size (nm)	17	18	8

4.3. SEM studies of materials

As can be seen in Fig. 17, the SEM images of ZFA, ZM3, ZC2 and MAG reveal non-uniformly sized particles. The particles form agglomerates which consist of irregularly shaped grains of various sizes, usually less than 500 nm. However some are as big as 1 μm and there is not a narrow distribution of particle sizes.

The original fly ash particles had a smooth surface because the surface is covered by an aluminosilicate glass phase [29]. By contrast, the surface of zeolitic materials is rough, indicating that zeolite crystals were deposited on the surface of underlying fly ash particles during the hydrothermal treatment.

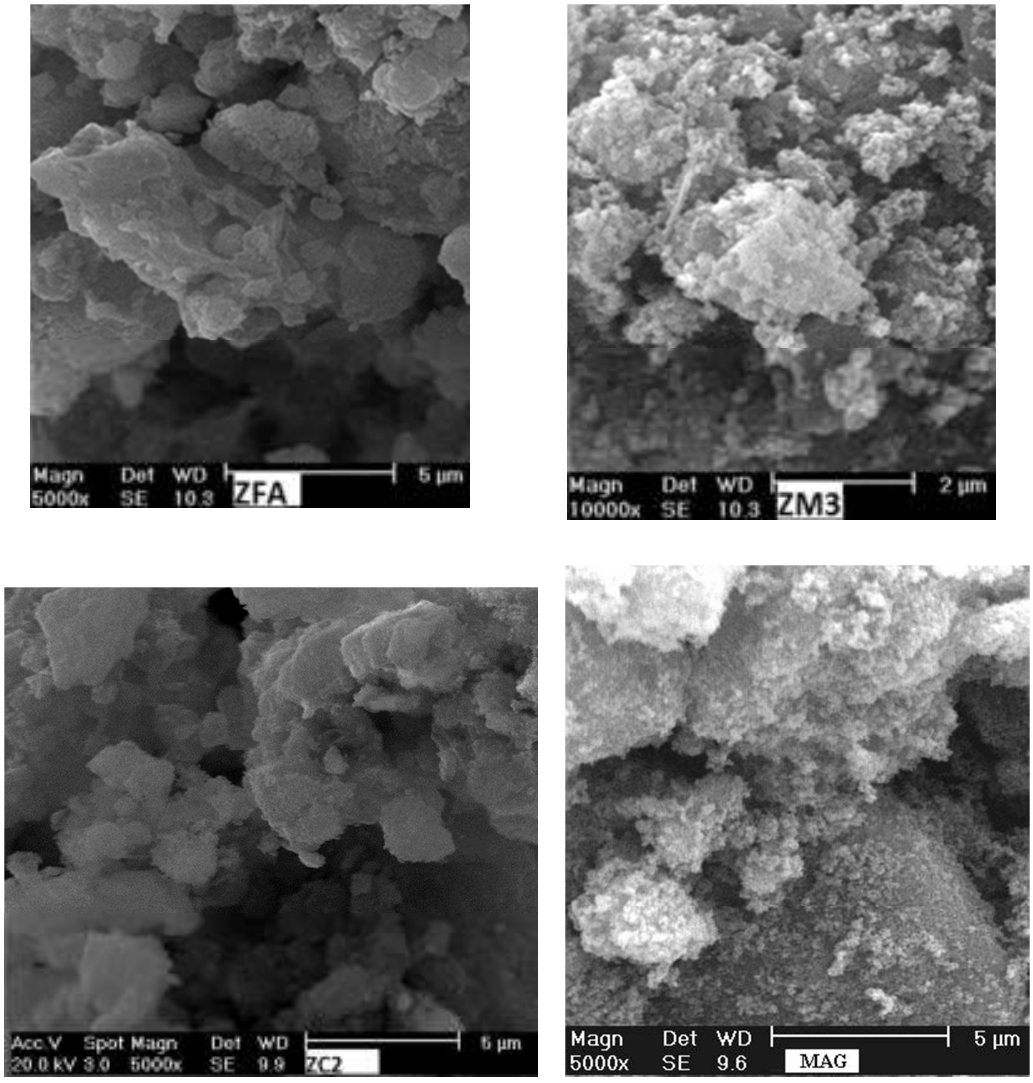

Figure 17. SEM images of zeolite from fly ash (ZFA), zeolite/Fe oxide composites (ZM3 and ZC2) and magnetite (MAG).

4.4. Magnetization measurements

The particle morphology and distribution of particle sizes can affect the magnetic properties such as residual magnetism. Among other effects, the response to magnetic force has been attributed to the size and shape of the particles.

Magnetic materials can retain a memory of an applied field once it is removed. This behavior is called hysteresis and a plot of the variation of magnetization with magnetic field is called a hysteresis loop.

The coercivity of fine particles has a strong dependence on the particle size. The decrease in coercivity with decreasing particle size in the single domain region is due to thermal effects. Below a critical diameter, the coercivity is zero because the thermal effects are strong enough to overcome the anisotropy energy and demagnetize the sample. Such particles are referred to as superparamagnetic and the hysteresis loop is not observed [64].

The magnetic properties of the zeolite/Fe oxide composites ZM3 and ZC2 were evaluated using a vibrating-sample magnetometer. The two powdered samples were subjected to magnetic measurements at 300 K cycling the field between ± 20 kOe and theirs magnetic properties were investigated on the obtained hysteresis loops shown in Fig. 18.

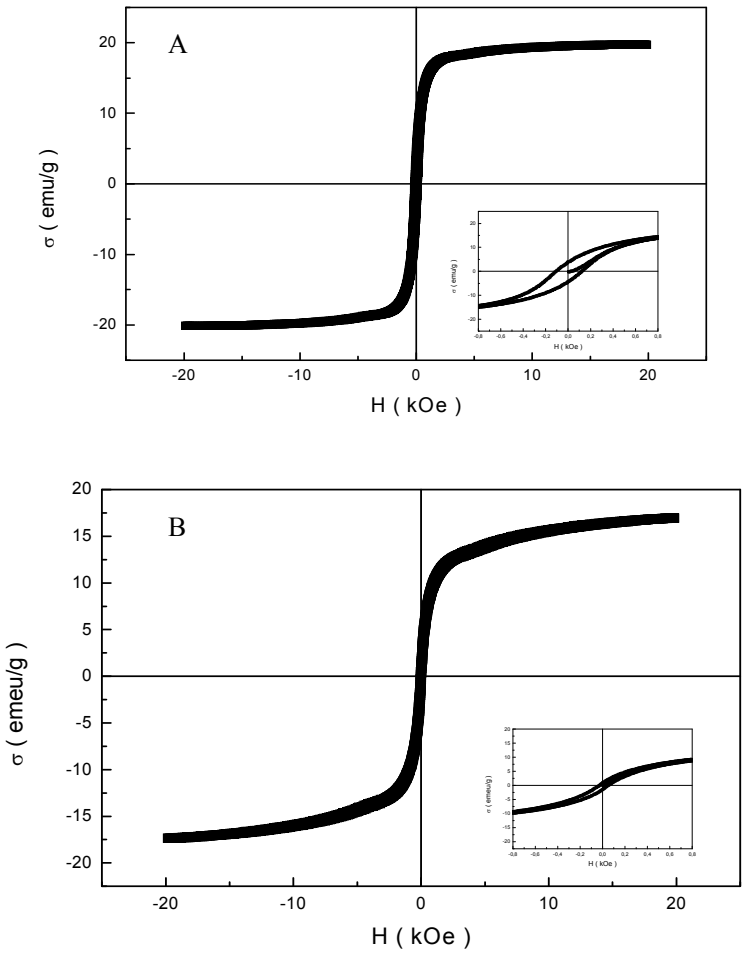

Figure 18. Magnetization loops measured at 300 K for the particles of (A) ZM3; (B) ZC2.

From the plot of magnetization (M) and magnetic field (H) and its enlargement near the origin, the very weak hysteresis revealed the resultant magnetic nanoparticles were nearly superparamagnetic with a saturation magnetization (Ms) of 19.9 and 19.7 emu g^{-1} for ZM3 and ZC2, respectively, at room temperature (300 K) and so that the average size of the particles is a few tens of nanometer which is in agreement with the XRD and SEM results.

As it was seen in the SEM images (Fig. 17), the samples are formed by grains of particles, so the result of the magnetic properties represents a total for all particles present in the cluster. The non-zero coercivity can be explained because the samples were more affected by the grain growth than by the reduction process and the formation of very fine grains.

This experiment proved that zeolite from fly ash-iron oxide nanocomposites possessed magnetism and could be potentially used as a magnetic adsorbents to remove compounds in liquid phase. As displayed in Fig. 19, the magnetic adsorbent can be removed from the liquid by applying an external magnetic field and re-dispersed (or resuspension) in another liquid medium after removal of the external magnetic field.

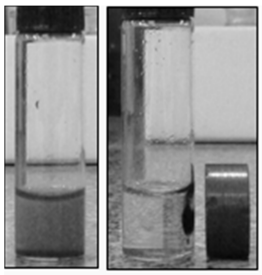

Figure 19. Separation of zeolite from fly ash-iron oxide composite from aqueous solution by a magnet after adsorption process.

4.5. FT-IR analysis

The FTIR spectra of the materials are given in Fig. 20. For MAG it is possible to visualize the absorption band of strong intensity at 568 cm^{-1} which can be assigned to the Fe-O stretching mode of the tetrahedral and octahedral sites of the magnetite [65].

The absorption bands in the range 992-456 cm^{-1} for ZFA were characterized as the infrared absorption bands of the zeolite hydroxysodalite [66]. The broad band at 992 cm^{-1} arises from the asymmetric stretch, ν_{as} (T-O-T, T = Si, Al). The bands located in the 775-653 cm^{-1} region are attributed to the symmetric stretch ν_s (T-O-T). The band around at 456 cm^{-1} is assigned to the bending vibration of δ(O-T-O). The broad band at 3431 cm^{-1} and a band at 1642 cm^{-1} can be related to the water molecules located inside the channels of zeolites and/or associated with exchangeable cations [67].

The FT-IR spectra (Fig. 20b) of zeolite-iron oxide composites ZM3 and ZC2 show the overlapping of the absorption bands of the zeolite from coal fly ash and magnetite particles. The appearance of a band of the Fe-O vibrations of the magnetite particles can be seen around 568-561 cm^{-1}.

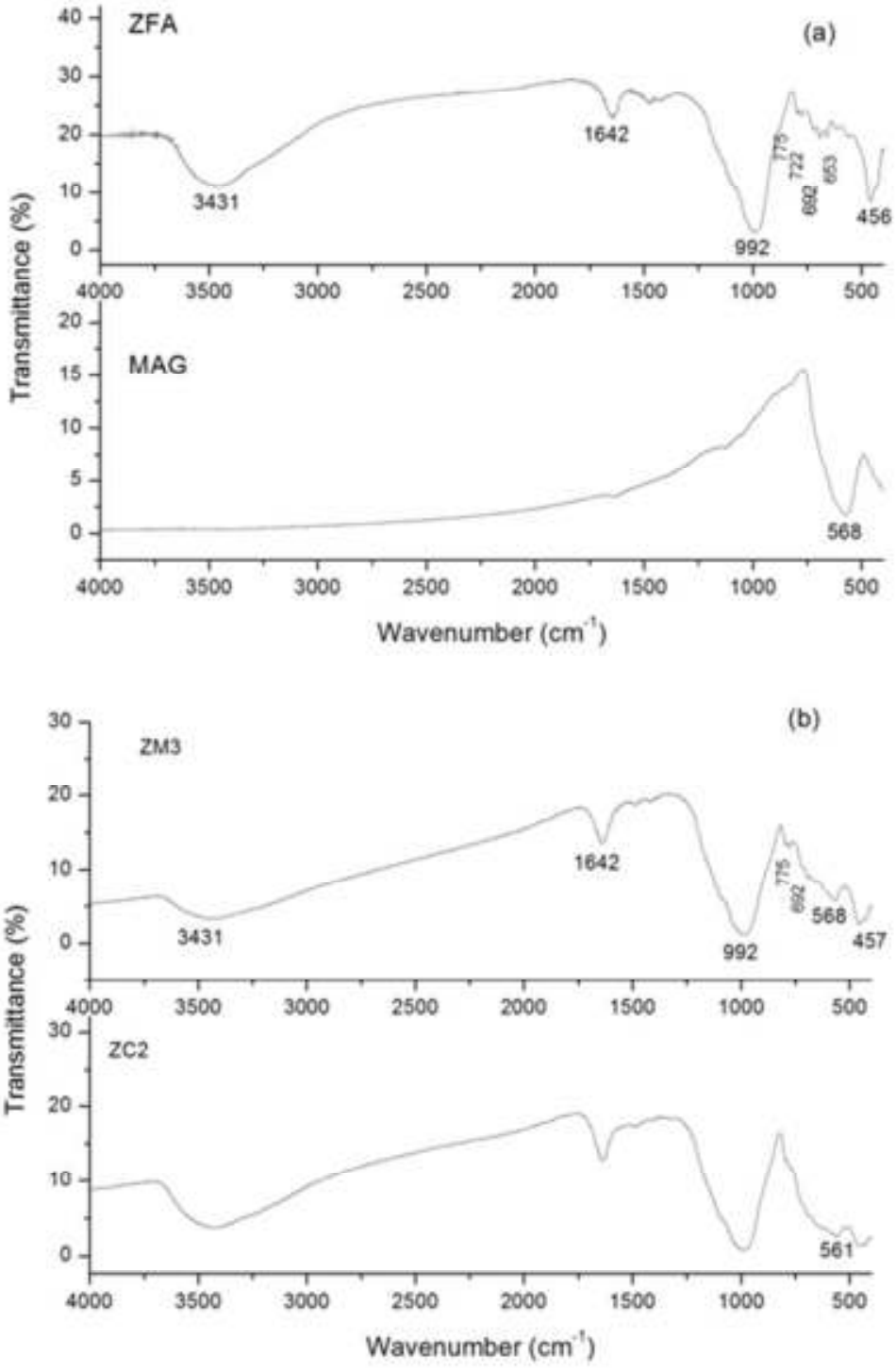

Figure 20. FTIR spectra of: (a) zeolite from fly ash (ZFA) and magnetite (MAG); (b) zeolite/Fe oxide composites (ZM3 and ZC2).

4. CONCLUSION AND FUTURE PERSPECTIVES

Zeolite synthesized from fly ash has a great potential in environmental applications and interesting alternative to replace natural and commercial zeolites for adsorption in water pollution treatment. Converting fly ash into zeolites not only alleviates the disposal problem but also converts a waste material into a marketable commodity.

Zeolite from fly ash-iron oxide nanocomposites were synthesized and investigated for the removal of dyes and toxic metals from aqueous solutions. A series of experiments were carried out in a batch adsorption technique to obtain the effect of process variables on adsorption.

The data obtained through this work support the view that the zeolite from fly ash-iron oxide nanocomposite is an effective low cost adsorbent for the removal of contaminants from aqueous solution.

If magnetic zeolite-iron oxide nanocomposite is used as the adsorbent for contaminants in water, magnetic separation will be applied and the clear solution could be easily decanted off or removed by pipette. Furthermore, supporting of magnetite nanoparticles on zeolitic material from coal fly ashes during the preparation process prevents the coaggregation of the iron oxide nanoparticles and is of help for their storage and pelletization.

Development of the adsorption process requires further investigation in the direction of testing zeolite from fly ash-iron oxide nanocomposites with real industrial effluents. Once batch conditions, characterization of adsorbents, adsorptive capacity and the uptake mechanism are investigated work should be done to design and carry out some pilot-plant scale studies to check their feasibility at industrial level.

The use of zeolite from fly ash-iron oxide nanocomposites for application in radioactive liquid waste treatment is also a promising prospect.

REFERENCES

[1] M. Yamaura, R. L. Camilo and M. C. F. C. Felinto, J. Alloys Compd. 344 (2002) 152.
[2] Z. H. Ai, Y. Cheng, L. Z. Zhang and J. R. Qiu, Environ. Sci. Technol. 42 (2008) 6955.
[3] S. Pal and E. C. Alocilja, Biosens. Bioelectron. 24 (2009) 1437.
[4] K. P. Singh, S. Gupta, A. K. Singh and S. Sinha, J. Hazard Mater. 186 (2011) 1462.
[5] I. Safarik, M. Safarikova and V. Buricova, Collect. Czech. Chem. Commun. 60 (1995) 1448.
[6] J. D. Orbell, L. Godhino, S. W. Bigger, T.M. Nguyen and L.N. Ngeh, J. Chem. Educ. 74 (1997) 1446.
[7] S. Y Mak, and D. H. Chen, Dyes Pigm. 61(2004) 93.
[8] P. Xianjia, L. Zhaokun, and Z. Hongmei, Chemosphere 63 (2006) 300.
[9] Q.L. Zhang, Y.C. Lin, X. Chen and N. Y. Gao, J. Hazard. Mater. 148 (2007) 671.
[10] P. Yuan, M. Fan, D. Yang, H. He, D. Liu, A. Yuan, J. Zhu and T. Chen, J. Hazard. Mater. 166 (2009) 821.
[11] G. S. Zhang, H. J. Liu, R. P. Liu and J. H. Qu, J. Colloid Interface Sci. 335 (2009) 168.
[12] Y Feng, J. L. Gonga, G. M. Zeng, Q. Y. Niu, H. Y. Zhang, C.G. Niu, J.H. Deng and M. Yan, Chem. Eng. J. 162 (2010) 487.

[13] L. C. A. Oliveira, D. I. Petkowics, A. Smaniott, and S. B. C. Pergher, Water Res. 38 (2004) 3699.
[14] L. C. A. Oliveira, R. V. R. A. Rios, J. D. Fabris, V. K. Garg, K. Sapag and R. M. Lago, Carbon 40 (2002) 2177.
[15] L. C. A. Oliveira, R. V. R. A. Rios, J. D. Fabris, K. Sapag, V. K. Garg and R. M. Lago, Appl. Clay Sci. (2003) 22 169.
[16] K. P. Singh, S. Gupta, A. K. Singh and S. Sinha, J. Hazard. Mater. **186** (2011) 1462.
[17] J. Levandowski and W. D. Kalkreuth, Int. J. Coal Geol. 77 (2009) 269.
[18] F. S. Depoi, D. Pozebon and W. D. Kalkreuth, Int. J. Coal Geol .76 (2008) 227.
[19] A. S. Meawad, D. Y. Bojinova and Y. G. Pelovski, Waste Manage 30 (2010) 2548.
[20] P. S. Polic, M. R. Ilic and A. R. Popovic, Handb. Environ. Chem. (2005) Doi:10.1007/b11733
[21] H. Holler and U. Wirsching, Fortschr. Miner. 63 (1985) 21.
[22] T. Henmi, Clay Sci. 6 (1987) 277.
[23] X. Querol, A. Alastuey, A. Lopez-Soler, J. M. Andres, R. Juan, P. Ferrer and C. R. Ruiz, Environ. Sci.Technol. 31 (1997) 2527.
[24] N. Shigemoto, H. Hayashi and K. Miyaura, J. Mater. Sci. 28 (1993) 4781.
[25] X. Querol, N. Moreno, J. C. Umaña, A. Alastuey, E. Hernández, A. López-Soler and F. Plana, Int. J. Coal Geol. 50 (2002) 413.
[26] S. S. Rayalu, A. K. Bansiwal, S. U. Meshram, N. Labhsetwar and S. Devotta, Catal. Sur. Asia 10 (2006) 74.
[27] D. A. Fungaro and J. E. A. Graciano, Adsorpt. Sci. Technol. 25 (2007) 729.
[28] D. A. Fungaro, M. Bruno and L. C. Grosche, Desalin. Water Treat. 2 (2009) 231.
[29] D. A. Fungaro, L. C. Grosche, A. S. Pinheiro, J. C. Izidoro and S. I. Borrely, Orbital Elec. J. Chem. 2 (2010) 235.
[30] D. A. Fungaro, M. Yamaura and T. E.M. Carvalho, J. At. Mol. Sci. 2 (2011) 305.
[31] T. E. M. Carvalho, D. A. Fungaro, C. P. Magdalena and P. Cunico, J. Radioanal. Nucl. Chem. 289 (2011) 617.
[32] Y. S. Ho and G. McKay, Can. J. Chem. Eng. 76 (1998) 822.
[33] Y. S. Ho, D. A. J. Wase, and C. F. Forster, Environ. Technol. 17 (1996) 71.
[34] W. J. Weber and J. C. Morris, J. Sanit. Engin. Div. ASCE 89 (1963) 31.
[35] I. Langmuir, J. Am.Chem. Soc. 40 (1918) 1361.
[36] H. M. F. Freundlich, J. Phys. Chem. 57 (1906) 385.
[37] K. R. Hall, L. C. Eagleton, A. Acrivos and T. Vermeulen, Ind. Eng. Chem. Fundam. 5 (1966) 212.
[38] Y. S. Ho, Carbon 42 (2004) 2115.
[39] Y. S. Ho, Water Res. 37 (2003) 2323.
[40] S. J. Allen, G. McKay and K. Y. H. Khader, Environ. Pollut. 56 (1989) 39.
[41] N. Dizge, C. Aydiner, E. Demirbas, M. Kobya, and S. Kara, J. Hazard. Mater. 150 (2008) 737.
[42] W. H. Cheung, Y. S. Szeto and G. McKay, Bioresour. Technol. 98 (2007) 2897.
[43] K. G. Bhattacharyya and A. Sharma, Dyes Pigm. 65 (2005) 51.
[44] W. A. Helby, Chem. Eng. 59 (1952) 153.
[45] B. Acemioglu, J. Colloid Int. Sci. 274 (2004) 371.

[46] G. Atun, G. Hisarlý, A. E. Kurtoglu, and N. Ayar, J. Hazard. Mater. 187 (2011) 562.
[47] A. Sharma and K. G. Bhattacharyya, Indian J. Chem. Technol. 12 (2005) 285.
[48] E. Gutierrez-Segura, M. Solache-Rios, and A. Colin-Cruz, J. Hazard. Mater. 170 (2009) 1227.
[49] M. B. Kasiri, H. Aleboyeh, and A. Aleboyeh, Appl. Catal. 84 (2008) 9.
[50] C. Namasivayam and R. T. Yamuna, Environ Pollut. 89 (1995) 1.
[51] C. Namasivayam, N. Muniasamy, K. Gayathri, M. Rani and K. Ranganathan, Biores Technol. 57 (1996) 37.
[52] C. Namasivayam, D. Prabha, and M. Kumutha, Bioresour. Technol. 64 (1998) 77.
[53] A. Shukla, Y. H. Zhang, P. Dubey, J. L. Margrave and S. S. Shukla , J. Hazard. Mater. 95 (2002) 137.
[54] B. Royer, N. F. Cardoso, E. C. Lima, V. S. O. Ruiz, T. R. Macedo and C. Airoldi, J. Colloid Interface Sci. 336 (2009) 398.
[55] C. H. Giles, T. H. MacEwan, S. N. Nakhwa, and D. Smith, J. Chemical Society (1960) 3973.
[56] C. Namasivayam and D. J. S. E. Arasi, Chemosphere, 34, 401 (1997).
[57] M. J. Zamzow and J. E. Murphy, Separ. Sci. Tech. 27 (1992) 1969.
[58] S. Kesraoui-Ouki, C. Cheeseman and R. Perry, Environ. Sci. Technol. 6 (1993) 1108.
[59] H. W. Sherry, *Ion exchange*, J. A. Manisky, ed.; Marcel Dekker, New York, cap. 2. (1969).
[60] S. K. Ouki and M. Kavannagh, Waste Manage. Res**.** 15 *(*1997) 383.
[61] G. Wulfsberg, *Principles of Descriptive Chemistry*, Brooks/Cole Publishing, Monterey, CA, p.2, (1987).
[62] W. Qiu and Y. Zheng, Chem. Eng. J. 145 (2009) 483.
[63] B. D. Cullity, *Elements of X-rays diffraction,* Addison Wesley Publishing Company, (1972).
[64] S. Gangopadhyay, G. C. Hadjipanayis, B. Dale, C. M. Sorensen and K. J. Klabunde, Nanostruct. Mater. 1 (1992) 77.
[65] J. Giri, S. Thakurta, J. Bellare, A. Nigam and D. Bahadur, J. Magn. Magn. Mater. 293 (2005) 62.
[66] C. Covarrubias, R. García, R. Arriagada, J. Yánez and M. T. Garland, Microp. Mesop. Mat. 88 (2006) 220.
[67] Th. Mouhtaris, D. Charistos, N. Kantiranis, A. Filippidis, A. Kassoli-Fournaraki and A. Tsirambidis, Microp. Mesop. Mat. 61 (2003) 57.